

A Geometric Approach to Pairwise Bayesian Alignment of Functional Data Using Importance Sampling

Sebastian Kurtek

*Department of Statistics
The Ohio State University
Columbus, OH*

e-mail: kurtek.1@stat.osu.edu

Abstract: We present a Bayesian model for pairwise nonlinear registration of functional data. We utilize the geometry of the space of warping functions to define appropriate prior distributions and sample from the posterior using importance sampling. A simple square-root transformation is used to simplify the geometry of the space of warping functions, which allows for computation of sample statistics, such as the mean and median, and a fast implementation of a k-means clustering algorithm. These tools allow for efficient posterior inference, where multiple modes of the posterior distribution corresponding to multiple plausible registrations of the given functions are found. We also show 95% credible intervals to assess the uncertainty of the alignment in different clusters. We validate this model on several simulated examples where the expected number of modes in the posterior distribution is known. We also present examples on real data from different application domains including biometrics and biology.

MSC 2010 subject classifications: Primary 62F15.

Keywords and phrases: functional data, Bayesian registration model, square root slope function, temporal alignment, warping function.

Contents

1	Introduction	2
1.1	Problem Background	2
2	Representation Space of Warping Functions	5
2.1	Statistics on Ψ	6
2.2	K-means Clustering on Ψ	7
3	Bayesian Registration Model	8
4	Importance Sampling	8
4.1	Implementation and Computational Cost	11
5	Exploring Multiple Modes in Posterior Distribution	11
6	Function Alignment Using Maximum a Posteriori Probability (MAP) Estimate	15
7	Summary and Future Work	18
	Acknowledgements	19
	References	19

1. Introduction

The problem of registration of functional data is important in many branches of science. In simple terms, it deals with deciding how points on one function match in some optimal way with points on another function. In contrast to landmark-based matching, such an approach matches the entire domains of the functions in a general registration problem. The study of registration problems is popular in image analysis where pixels or voxels across images are matched, and in shape analysis of objects where points across shapes are matched. One can broadly classify registration problems into two main groups: (1) pairwise registration and (2) groupwise registration. In pairwise registration, one solves for an optimal matching between two objects, while in groupwise registration multiple (> 2) objects are simultaneously registered. In this paper, we are focused on the problem of pairwise registration. This problem has been referred to in many different ways, some of which are alignment, warping, deformation matching, phase removal, and so on. While registration can be studied for many types of objects, from simple functions to complex high-dimensional objects, the fundamental issues in registration are often similar. We will focus on perhaps the simplest objects for studying registration problems, \mathbb{R} -valued functions on $[0, 1]$. More specifically, we will take a Bayesian approach to this problem and compare it to past ideas that often take an optimization-based approach. We will define a parameter space of the registration variable, denoted by γ , define a prior model on that space, and use that prior to generate Bayesian inferences.

There exists a large literature on statistical analysis of functions, in part due to the pioneering efforts of [17], [7], and several others [14, 22]. When restricting to the analysis of elastic functions (functions that are temporally aligned) the literature is relatively recent and limited [16, 5, 14, 6, 22, 8]. The general approach in all of these methods is to use an energy function to compute optimal registrations and perform subsequent analysis on the aligned functions using standard tools from functional data analysis such as the cross-sectional mean, covariance and functional Principal Component Analysis (fPCA). More recently, there is also growing literature on registration methods that are based on Bayesian principles. Telesca and Inoue [23] proposed a semi-parametric model for multiple alignment of functional data. These models were further extended in the context of analyzing microarray data in [24]. A non-parameteric approach to the multiple registration problem was proposed recently in [21]. A different Bayesian model was proposed for registering liquid chromatography-mass spectrometry data in [25]. The main limitation of most methods in current literature is the choice of metric used for registration and subsequent analysis. One exception is the hierarchical Bayesian registration model presented by [2]. We elaborate on these issues next.

1.1. Problem Background

Before we describe our Bayesian framework, we first setup the registration problem mathematically. Let \mathcal{F} be an appropriate subset (made precise later) of

real-valued functions on the interval $[0, 1]$. For any two functions $f_1, f_2 \in \mathcal{F}$, the registration problem is defined as finding the mapping γ such that point $t \in [0, 1]$ in the domain of f_1 is matched to the point $\gamma(t)$ in the domain of f_2 . In other words, the functions $f_1(t)$ and $f_2(\gamma(t))$ are optimally matched under the chosen optimality criterion. The main question that arises is: What should be the criterion for optimal registration? A natural tendency is to choose an \mathbb{L}^p -norm between f_1 and $f_2 \circ \gamma$, but there are some known limitations of that approach. For instance, if we choose the \mathbb{L}^2 norm, defined as $\|f_1 - f_2\| = \sqrt{\int_0^1 |f_1(t) - f_2(t)|^2 dt}$, we obtain the following optimization problem:

$$\gamma^* = \arg \inf_{\gamma} \|f_1 - f_2 \circ \gamma\|. \quad (1)$$

This setup can lead to a degenerate solution, termed the *pinching effect*. In this case, one can pinch the entire function f_2 to get arbitrarily close to f_1 in \mathbb{L}^2 norm. To avoid this situation, one often adds a roughness penalty on γ , denoted by $\mathcal{R}(\gamma)$, leading to the optimization problem $\inf_{\gamma} (\|f_1 - f_2 \circ \gamma\|^2 + \lambda \mathcal{R}(\gamma))$. Although this avoids the pinching effect, it introduces some other issues. Firstly, the choice of λ is not obvious in general cases. Secondly, and more importantly, this solution is not symmetric. That is, the optimal registration of f_1 to f_2 can be quite different from that of f_2 to f_1 . Another related issue is that this criterion is not a proper metric and this leads to additional problems in later analysis. Most of the past papers on registration of functional data involve this setup and inherit the above-mentioned limitations.

In order to handle these issues, Srivastava et al. [20, 10] proposed a novel approach that has its foundations in differential geometry. First, let the set of all registration or warping functions be defined as $\Gamma = \{\gamma : [0, 1] \rightarrow [0, 1] | \gamma(0) = 0, \gamma(1) = 1, 0 < \dot{\gamma} < \infty\}$. Γ forms a group under the composition map, i.e. for any $\gamma_1, \gamma_2 \in \Gamma$, their composition $\gamma_1 \circ \gamma_2$ is also in Γ and for any $\gamma \in \Gamma$, there is a unique $\gamma^{-1} \in \Gamma$. The $\gamma_{id}(t) = t$ is the identity element of this group. The next item is to represent the given functions by their square-root slope functions (SRSFs): $q(t) = \text{sign}(\dot{f}(t))\sqrt{|\dot{f}(t)|}$. For registration analysis in this approach, each $f \in \mathcal{F}$ is represented by its SRSF q . One sets \mathcal{F} to be the space of all absolutely continuous functions and the resulting space of all SRSFs is $\mathbb{L}^2([0, 1], \mathbb{R})$ henceforth referred to simply as \mathbb{L}^2 . For every $q \in \mathbb{L}^2$ there exists a function f (unique up to a constant) such that the given q is the SRSF of that f . In fact, this function can be obtained precisely using the equation $f(t) = f(0) + \int_0^t q(s)|q(s)|ds$. Note that if a function f is warped by γ to $f \circ \gamma$, its SRSF changes from q to $(q, \gamma) = (q \circ \gamma)\sqrt{\dot{\gamma}}$; this last term involving $\sqrt{\dot{\gamma}}$ is an important departure from previous solutions. To setup the registration problem, we define an equivalence class of an SRSF as $[q] = \{(q, \gamma) | \gamma \in \Gamma\}$. Finally, the pairwise registration between any two functions f_1 and f_2 is performed by solving an optimization problem over equivalence classes of their SRSF representations:

$$\gamma_{DP} = \arg \inf_{\gamma \in \Gamma} \|q_1 - (q_2, \gamma)\|. \quad (2)$$

The solution to this problem is computed using the dynamic programming (DP)

algorithm. The resulting distance between f_1 and f_2 is then given by:

$$d([q_1], [q_2]) = \|q_1 - (q_2, \gamma_{DP})\|. \quad (3)$$

As described in [20], this framework has many advances: it avoids the pinching problem, its registration solution is symmetric, it does not require an additional regularization term and the choice of λ that goes with it, and it is actually a proper metric in the quotient space \mathcal{F}/Γ which provides an important tool for ensuing analysis. The most important reason why this setup avoids many problems of Equation 1 is that $\|q_1 - q_2\| = \|(q_1, \gamma) - (q_2, \gamma)\|$ for any $\gamma \in \Gamma$. In mathematical terms, it means that the action of Γ on \mathbb{L}^2 is by isometries. This method was also later extended to apply to statistical analysis of cyclostationary biosignals [12] and was shown to perform well in different applications [26, 27, 29].

Recently, it has been argued that a Bayesian approach rather than pure optimization is a better option for many situations. The advantages of this approach include a comprehensive exploration of the variable space, Γ , resulting in potential multimodal solutions to the registration problem. This framework, like any Bayesian solution, also allows for computing confidence values associated with the estimates. The difficulty lies in defining an appropriate prior on Γ , or some relevant subset, to enable efficient Bayesian inference. Cheng et al. [2] used the SRSF representation of functional data and utilized the fact that $\dot{\gamma}$ is a probability density function. In this way, they constructed a Dirichlet process to impose a prior model implicitly on Γ and sampled from the posterior distribution using Markov Chain Monte Carlo techniques. In this paper, we describe a very convenient geometric structure, a unit sphere, using the square-root density (SRD) representation of γ and use its geometry to impose priors on high-dimensional spheres. In this setup, we develop a Bayesian registration model and utilize importance sampling to sample from the posterior and compute posterior functionals such as the mean, median or maximum a posteriori probability (MAP) estimate. We also provide pointwise standard deviations and credible intervals to assess alignment uncertainty. We show that these tools are especially effective when two or more registrations are plausible. *We note that the spherical geometry of the space of warping functions Γ in conjunction with importance sampling has not been previously explored for Bayesian pairwise alignment of functional data.*

The rest of this paper is organized as follows. In Section 2, we describe tools for statistical analysis on Γ . In Section 3, we introduce our registration model and in Section 4 we describe an importance sampling approach for sampling from the posterior distribution of warping functions. Finally, in Sections 5 and 6, we present different experimental results including ones where the posterior distribution is multimodal. We also compare some of our results to a Bayesian nonparametric approach via importance sampling using the Dirichlet process. Finally, we close with a brief summary and directions for future work in Section 7.

2. Representation Space of Warping Functions

The proposed hierarchical model utilizes prior distributions and importance functions on the space of warping functions Γ . Thus, we are faced with defining statistics and probability distributions on this space. In order to do this we use the Fisher-Rao Riemannian metric on Γ , which is given by (for $w_1, w_2 \in T_\gamma(\Gamma)$ and $\gamma \in \Gamma$) $\langle w_1, w_2 \rangle_\gamma = \int_0^1 \dot{w}_1(t) \dot{w}_2(t) \frac{1}{\dot{\gamma}(t)} dt$ [18, 19, 9], where \dot{w} and $\dot{\gamma}$ represent time derivatives. An important property of the Fisher-Rao metric is that it is invariant to re-parameterizations of probability density functions [28]. While this is not the only metric that achieves this property, it is important to note that there is no invariant metric that does not include derivatives. It is possible to define statistics and probability models directly on Γ under the Fisher-Rao metric, but this proves to be very complicated due to the non-trivial Riemannian geometry of this space.

Inference on Γ is greatly simplified using a convenient transformation, which is similar to the definition of the SRSF for general functions.

Definition 1. Define the mapping $\phi : \Gamma \rightarrow \Psi$. Then, given an element $\gamma \in \Gamma$, define a new representation $\psi : [0, 1] \rightarrow \mathbb{R}_{\geq 0}$ using the square-root of its derivative as $\phi(\gamma) = \psi = \sqrt{\dot{\gamma}}$.

This is the same as the SRSF defined earlier for functions and takes this form because $\dot{\gamma} > 0 \forall t$. For simplicity and to distinguish it from the SRSF representation of functions, we refer to this representation as the square-root density (SRD). The identity map $\gamma_{id}(t) = t$ maps to a constant function with value $\psi_{id}(t) = 1$. An important advantage of this transformation is that the \mathbb{L}^2 norm of a function ψ is 1, i.e. $\|\psi\|^2 = \int_0^1 \psi(t)^2 dt = \int_0^1 \dot{\gamma}(t) dt = \gamma(1) - \gamma(0) = 1$. Thus, the set of all such ψ s, denoted by Ψ , is a subset of the unit sphere in \mathbb{L}^2 . The tangent space for all ψ that are not on the boundary of Ψ is defined as $T_\psi(\Psi) = \{v : [0, 1] \rightarrow \mathbb{R} | \langle v, \psi \rangle = 0\}$, where $\langle \cdot, \cdot \rangle$ is the standard \mathbb{L}^2 inner product. Furthermore, as shown in [1, 18, 19, 9], the Fisher-Rao metric on the space of time warping functions simplifies to the \mathbb{L}^2 metric on Ψ , which in turn greatly simplifies all computation. Given a function ψ one can easily compute the corresponding warping function via integration using $\gamma(t) = \int_0^t \psi(s)^2 ds$; this provides the inverse mapping $\phi^{-1} : \Psi \rightarrow \Gamma$. Thus, the geodesic path between two warping functions, $\gamma_1, \gamma_2 \in \Gamma$ represented using their SRDs $\psi_1, \psi_2 \in \Psi$, is simply the great circle connecting them ($\alpha : [0, 1] \rightarrow \Psi$), $\alpha(\tau) = \frac{1}{\sin(\theta)} [\sin(\theta - \theta\tau)\psi_1 + \sin(\theta\tau)\psi_2]$, where θ represents the length of this path (geodesic distance between warping functions γ_1 and γ_2 under the Fisher-Rao metric) and is simply the arc-length between ψ_1 and ψ_2 :

$$d(\gamma_1, \gamma_2)_{FR} = d(\psi_1, \psi_2) = \theta = \cos^{-1}(\langle \psi_1, \psi_2 \rangle). \quad (4)$$

Since the differential geometry of the sphere is well known, this transformation also simplifies the problem of defining probability distributions of warping functions. The general approach will be to define wrapped probability distributions, and perform random sampling and probability calculations on Ψ . In order

to achieve this goal, we must first define some standard tools from differential geometry for this space. We begin by providing the definition of the exponential and inverse exponential maps. For $\psi \in \Psi$ and $v \in T_\psi(\Psi)$, the exponential map is defined as $\exp : T_\psi(\Psi) \rightarrow \Psi$ by $\exp_\psi(v) = \cos(\|v\|)\psi + \frac{\sin(\|v\|)}{\|v\|}v$. For $\psi_1, \psi_2 \in \Psi$, the inverse exponential map is defined as $\exp^{-1} : \Psi \rightarrow T_\psi(\Psi)$ by $\exp_{\psi_1}^{-1}(\psi_2) = \frac{\theta}{\sin(\theta)}(\psi_2 - \cos(\theta)\psi_1)$. These two expressions provide a natural way of mapping points from the representation space Ψ to the tangent space (at a particular element of Ψ) and vice versa. Another tool from differential geometry that is useful in defining probability models on the space of warping functions is parallel transport. This tool transports tangent vectors along paths on a Riemannian manifold. We use the parallel transport along geodesic paths (in this case great circles on the sphere) to define an orthonormal basis in the tangent space at any point on Ψ by transporting a standard basis defined on the tangent space at the identity element, $T_1(\Psi)$. For $\psi_1, \psi_2 \in \Psi$, the shortest geodesic path $\alpha : [0, 1] \rightarrow \Psi$ such that $\alpha(0) = \psi_1$ and $\alpha(1) = \psi_2$, and a vector $v \in T_{\psi_1}(\Psi)$, its parallel transport along α to ψ_2 is defined as $w = v - \frac{2\langle v, \psi_2 \rangle}{\|\psi_1 + \psi_2\|}(\psi_1 + \psi_2)$. This defines a mapping $\kappa : T_{\psi_1}(\Psi) \rightarrow T_{\psi_2}(\Psi)$ such that $w = \kappa(v)$. An important property of parallel transport is that the mapping κ is an isometry between the two tangent spaces, i.e. for $v_1, v_2 \in T_{\psi_1}(\Psi)$, $\langle v_1, v_2 \rangle = \langle \kappa(v_1), \kappa(v_2) \rangle$.

Discretization: In order to apply the proposed methodology we discretize the functional data and the warping functions using a dense sampling of N points: $t = \{t_1, \dots, t_N\} \in [0, 1]$, where N depends on the application of interest. We have found through numerous experiments that $N = 100$ is usually sufficient. This allows us to model differences between SRSFs using finite Gaussian processes and to define prior probability models on the space of warping functions using multivariate, wrapped Gaussian distributions. In addition, we use a discrete approximation to compute the quantities defined in Sections 1.1 and 2.

2.1. Statistics on Ψ

In addition to defining prior distributions on the space of warping functions, we would like to be able to compute summary statistics such as the mean or median. These tools are especially useful in inference based on samples generated from the posterior distribution. Suppose that we have a sample of warping functions $\gamma_1, \dots, \gamma_p$. To begin, we are interested in defining a mean and median of these functions. To do this we again exploit the geometry of Ψ . We begin by mapping all of the functions γ to their corresponding SRD representations resulting in ψ_1, \dots, ψ_p . Once this is done, all of our data is on the subset of the unit sphere, where the geodesic distance is used to compute their intrinsic mean and median as follows. The sample Karcher mean is given by $\bar{\psi} = \operatorname{argmin}_{\psi \in \Psi} \sum_{i=1}^p d(\psi, \psi_i)^2$. Similarly, the sample median of the functions is defined as $\tilde{\psi} = \operatorname{argmin}_{\psi \in \Psi} \sum_{i=1}^p d(\psi, \psi_i)$. A gradient-based approach for finding the Karcher mean and median are given in several places [13, 3, 4, 11], and are repeated here for convenience for the space of interest Ψ .

Algorithm 1. (Karcher Mean): Let $\bar{\psi}_0$ be an initial estimate of the Karcher mean. Set $j = 0$ and ϵ_1, ϵ_2 to be small positive values.

- (1) For each $i = 1, \dots, p$, compute $v_i = \exp_{\bar{\psi}_j}^{-1}(\psi_i)$.
- (2) Compute the average direction $\bar{v} = \frac{1}{p} \sum_{i=1}^p v_i$.
- (3) If $\|\bar{v}\| < \epsilon_1$, then stop. Else, update using $\bar{\psi}_{j+1} = \exp_{\bar{\psi}_j}(\epsilon_2 \bar{v})$.
- (4) Set $j = j + 1$ and return to Step 1.

Algorithm 2. (Geometric Median): Let $\tilde{\psi}_0$ be an initial estimate of the median. Set $j = 0$ and ϵ_1, ϵ_2 to be small positive values.

- (1) For each $i = 1, \dots, p$, compute $v_i = \exp_{\tilde{\psi}_j}^{-1}(\psi_i)$ and $d_i = d(\tilde{\psi}_j, \psi_i)$.
- (2) Compute the update direction $\tilde{v} = \sum_{i=1}^p \frac{v_i}{d_i} (\sum_{i=1}^p \frac{1}{d_i})^{-1}$.
- (3) If $\|\tilde{v}\| < \epsilon_1$, then stop. Else, update using $\tilde{\psi}_{j+1} = \exp_{\tilde{\psi}_j}(\epsilon_2 \tilde{v})$.
- (4) Set $j = j + 1$ and return to Step 1.

2.2. K-means Clustering on Ψ

One of the motivations behind this work is the discovery and analysis of multiple modes in the posterior distribution of warping functions. For this purpose, we introduce a k-means clustering approach on Ψ . In the previous section, we have defined a procedure to compute the Karcher mean of warping functions and we will use it to specify the k-means clustering algorithm. Let $\gamma_1, \dots, \gamma_p$ be a sample from the posterior distribution and ψ_1, \dots, ψ_p be their corresponding SRD representations. The k-means clustering computes a partition of the sample space such that the within cluster sum of squared distances is minimized. This is achieved using the following standard algorithm [15]:

Algorithm 3. (K-Means): To initialize, choose k unique functions $\bar{\psi}_{1,0}, \dots, \bar{\psi}_{k,0}$ from the set $\{\psi_1, \dots, \psi_p\}$ and set $j = 0$.

- (1) For each $i = 1, \dots, p$ and $m = 1, \dots, k$, compute $d_{i,m} = d(\bar{\psi}_{m,j}, \psi_i)$ using Equation 4.
- (2) Assign each function ψ_i , $i = 1, \dots, p$, to the cluster which minimizes $d_{i,\cdot}$.
- (3) Update cluster means $\bar{\psi}_{1,j+1}, \dots, \bar{\psi}_{k,j+1}$ using Algorithm 1.
- (4) Set $j = j + 1$.
- (5) Repeat Steps 1-4 until cluster assignments remain unchanged.

There are two main limitations of this algorithm: (1) the solution strongly depends on the initialization of the k cluster means and (2) the number of clusters k must be specified a priori (usually the expected number of posterior modes is not known). We address these two issues in our algorithm using hierarchical distance based clustering as follows. First, we compute all pairwise distances between the given samples using Equation 4. Then, we perform hierarchical clustering using the maximum linkage criterion, and visualize the generated clusters using a dendrogram. Based on the dendrogram, we choose the number of clusters k that is used in the k-means clustering algorithm. We also use the hierarchical clustering results to initialize the k means. A major benefit of this algorithm is its flexibility. One can easily replace the k -means formulation by,

for example, k -medians. This is especially useful when the mean may not be a good estimate of the posterior mode of interest.

3. Bayesian Registration Model

Given two functions f_1, f_2 and their corresponding SRSFs q_1, q_2 , we introduce a novel Bayesian model for function registration. At the first stage, we model the difference $q_1 - (q_2 \circ \phi^{-1}(\psi))\psi|\psi$ using a discrete time Gaussian process. This part of our model is exactly the same as that proposed in [2]. That is,

$$q_1 - (q_2 \circ \phi^{-1}(\psi))\psi|\psi \sim N(0, \sigma_1^2 I_N) \text{ (likelihood denoted by } L). \quad (5)$$

The second stage of our model places a prior distribution on the space of time warping functions Γ by utilizing their SRD representation:

$$\psi \sim WN(\mu_\psi, \Sigma_\psi) \text{ (denoted by } \pi). \quad (6)$$

We set the mean of the prior to be the identity mapping $\mu_\psi = 1$, which provides natural regularization toward γ_{id} (no warping). Thus, the prior distribution π is a wrapped normal distribution defined and evaluated in $T_1(\Psi)$. To define the covariance structure, we require an orthonormal basis in the tangent space $T_1(\Psi)$. It is easily verified that $\tilde{B} = \{\sqrt{2}\sin(2\pi jt), \sqrt{2}\cos(2\pi jt)|j = 1, 2, \dots, n\}$ forms an orthonormal basis for this tangent space under the \mathbb{L}^2 metric. This basis is truncated by choosing a maximum number $j = n$, which yields $2n$ basis elements. The truncation of the basis is important for additional regularization (smoothness of the warping functions) and computational efficiency. This, in turn, enables us to define a diagonal covariance matrix in terms of the basis as $\Sigma_\psi = \tilde{B}^T K_1 \tilde{B}$, where $K_1 = \sigma_2^2 I_{2n}$ is a diagonal covariance matrix with a large value for σ_2^2 ; thus, we assume a non-informative prior distribution where all directions of variation are equally likely. The wrapped normal prior is then defined as follows:

$$\pi(\psi|1, K_1) \propto \exp\left(-\frac{1}{2} \exp_1^{-1}(\psi) \tilde{B}^T K_1^{-1} \tilde{B} \exp_1^{-1}(\psi)^T\right). \quad (7)$$

Under this specification of the model, the posterior distribution of ψ becomes:

$$f(\psi|q_1, q_2) \propto L(q_1 - (q_2 \circ \phi^{-1}(\psi))\psi|\psi) \pi(\psi). \quad (8)$$

In order to sample from the posterior distribution and perform Bayesian inference we will utilize importance sampling on Ψ .

4. Importance Sampling

We begin by briefly introducing the concept of importance sampling and then provide some details of how this can be applied to our problem. Importance sampling is a variance reduction technique in Monte Carlo estimation where instead

of directly sampling from a distribution of interest, which may be inefficient, one first samples from an importance function and then re-samples based on appropriate weights. Suppose that we are interested in estimating the value of the following integral: $\theta = \int_{\mathcal{X}} g(x)f(x)dx$, where $f(x)$ is a probability density function. The classical Monte Carlo estimate of this integral is given by $\hat{\theta} = \sum_{i=1}^S g(x_i)$, where $\{x_1, \dots, x_S\}$ are samples from f . If the variance of the classical Monte Carlo estimate is large it may be beneficial to introduce a new function h , termed the *importance function*, which can be used to generate the samples instead of f . One can then rewrite the integral as $\theta = \int_{\mathcal{X}} \frac{g(x)f(x)}{h(x)}h(x)dx$. The improved Monte Carlo estimate becomes $\tilde{\theta} = \sum_{i=1}^S g(x_i)w(x_i)$, where $\{x_1, \dots, x_S\}$ are samples from h and $w(x) = \frac{f(x)}{h(x)}$. We use this idea to generate samples from the posterior distribution represented by f as follows. Given a large sample $\{x_1, \dots, x_S\}$ from h , we compute the associated weights as $\{\frac{f(x_1)}{h(x_1)}, \dots, \frac{f(x_S)}{h(x_S)}\}$. Then, to obtain s samples from f (where s is generally much smaller than S), we re-sample the set $\{x_1, \dots, x_S\}$ with the corresponding (normalized) weights with replacement. This provides a flexible and efficient methodology for sampling from the posterior distribution. This process is also called sampling importance resampling.

For our problem, we are faced with defining an importance function h that allows us to efficiently sample from f . The main requirement on h is that its support is the same as f . One option is to use the prior as the importance function directly and generate the weights using the likelihood. But, in other cases, one may want to “upsample” a different part of the space, i.e. near the dynamic programming solution. Thus, we provide a general recipe for constructing wrapped Gaussian importance functions similar to the definition of the prior. In order to do this, we require a method for defining an orthonormal basis in the tangent space at any point on Ψ . Given the truncated basis \tilde{B} in $T_1(\Psi)$ defined in the previous section, we can define an orthonormal basis in the tangent space at an arbitrary point $T_{\mu_\psi}(\Psi)$ using parallel transport, which was defined in Section 2. Parallel transport defines an isometric mapping between tangent spaces, and thus preserves the lengths of the basis vectors and the angles between them. We refer to the orthonormal basis in $T_{\mu_\psi}(\Psi)$ as B and use it to define a coordinate system in that space. This, in turn, enables us to define the covariance matrix as $\Sigma_\psi = B^T K B$, where K is diagonal with σ_3^2/j as its j th diagonal element. This is slightly different from the covariance structure in the prior because, in practice, we want to favor sampling of smoother warping functions; thus, we weigh the low frequency basis elements (corresponding to low values of j) higher than the high frequency basis elements. In this way we can define a general version of the importance function as:

$$h(\psi|\mu_\psi, K) \propto \exp\left(-\frac{1}{2} \exp_{\mu_\psi}^{-1}(\psi) B^T K^{-1} B \exp_{\mu_\psi}^{-1}(\psi)^T\right). \quad (9)$$

Figure 1 provides a pictorial explanation of our definition of the wrapped normal importance sampling density in the tangent space. Given this setup we can generate random samples from h in the tangent space using $v_{rnd} = \sum_{j=1}^{2n} z_j \sqrt{K_{jj}} B_j$

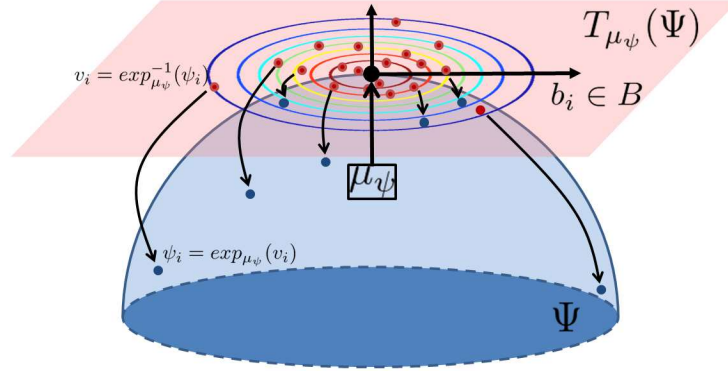


FIG 1. We define wrapped normal densities in the tangent space at a pre-specified mean. We utilize these models as priors and importance functions on the space of warping functions. One can generate random samples from the Gaussian model on the tangent space and then use the exponential map to get a random warping function.

where $z_j \stackrel{iid}{\sim} N(0, 1)$. B_j denotes the j th row of B (j th basis element) and K_{jj} denotes the j th diagonal element of the matrix K . v_{rnd} can be mapped to Ψ using $\psi_{rnd} = \exp_{\mu_\psi}(v_{rnd})$.

Using the idea of importance sampling, we can re-write the posterior distribution as follows:

$$f(\psi|q_1, q_2) \propto \frac{L(q_1 - (q_2 \circ \phi^{-1}(\psi))\psi|\psi)\pi(\psi)h(\psi)}{h(\psi)}. \quad (10)$$

Thus, our approach is to generate a large sample $\{\psi_1, \dots, \psi_S\}$ from h and evaluate a weight for each sampled warping function using:

$$\begin{aligned} \eta_i &= \frac{L(q_1 - (q_2 \circ \phi^{-1}(\psi_i))\psi_i|\psi_i)\pi(\psi_i)}{h(\psi_i)} \\ &\propto \exp\left(-\frac{1}{2\sigma_1^2}\|q_1 - (q_2 \circ \psi^{-1}(\psi_i))\psi_i\|^2 - \frac{1}{2}\exp_1^{-1}(\psi)\tilde{B}^T K_1^{-1}\tilde{B}\exp_1^{-1}(\psi)^T\right. \\ &\quad \left.+ \frac{1}{2}\exp_{\mu_\psi}^{-1}(\psi)B^T K^{-1}B\exp_{\mu_\psi}^{-1}(\psi)^T\right), \quad i = 1, \dots, S. \end{aligned} \quad (11)$$

Once all of the weights have been computed, we normalize them to $\tilde{\eta}_i = \frac{\eta_i}{\sum_{i=1}^S \eta_i}$. We then resample, with replacement, a small number s of ψ s from the original set. The resampled functions ψ_1, \dots, ψ_s are samples from the posterior distribution f , and can be mapped to their corresponding warping functions using ϕ^{-1} . Posterior functionals can be mapped to Γ in the same way. Note that it is obvious from the expression in Equation 11, that in the special case when the importance sampling function is the same as the prior (that is, $\mu_\psi = 1$ and $K = K_1$), one can simply sample from the prior distribution and weight each sample using the likelihood.

4.1. Implementation and Computational Cost

There are multiple parameters that we specify at the implementation stage. In most examples, we initially sample the functions with 100 points. We have found that this is a dense enough sampling to implement this methodology. Additionally, we rescale all of the functions such that $\|q\|^2 = 1$. As shown by [20], a major benefit of the metric introduced in Section 1.1 is that estimating γ is independent of amplitude scales of the given functions. Re-scaling the functions improves computational stability and allows us to fix the variance in the likelihood to be the same for all examples. Although we could specify an additional prior for the parameter σ_1^2 and a hyperprior for σ_2^2 , we pre-specify them to be $\sigma_1^2 = 0.09$ and $\sigma_2^2 = 1000$, which we have found to work well in practice. This step also significantly reduces our computational burden. Finally, we use $\sigma_3^2 = 1000$ and a total of 20 basis elements to sample from the importance function and evaluate the prior. We use the importance function to generate 100000 original samples. We then re-sample 300 of these functions with the appropriate weights. The overall computational cost of the importance sampling portion of this method is approximately 30 seconds (on average) on a Dell Desktop with an Intel Core i7 processor.

We compare some of the simulated data results to using a Dirichlet process prior with the same likelihood function. In all of the presented results, we set the parameters of the Dirichlet distribution $\alpha_1, \dots, \alpha_{40} = 1$. In this case, we again use importance sampling to generate samples from the posterior distribution, but we simply use the prior distribution as the importance function. The weights for each sample are then proportional to the likelihood. This setup is very similar to [2] but they utilize MCMC to generate samples from the posterior. The computational cost in this case is approximately 50 seconds (on average) on the same machine. We are unaware of the computational cost of the MCMC technique given in [2].

5. Exploring Multiple Modes in Posterior Distribution

One of the goals of this paper is to discover multiple plausible registrations of two functions based on the modes of the estimated posterior distribution. In this section, we provide results on simulated and real data where the multiple modes of the posterior distribution are discovered using k-means clustering. A main disadvantage of using k-means clustering is that the number of posterior modes, which is not usually known, must be pre-specified. While it would be much better to find the number of modes in addition to the clusters, this is a difficult problem and is beyond the scope of this work. In all examples presented in this section, the posterior samples are generated using importance sampling, where the importance function is centered at γ_{id} . We compute the mean ($\bar{\gamma}$), median ($\tilde{\gamma}$) and MAP (γ_{MAP}) estimate of the warping functions based on the clustered posterior samples, and compare some of the simulated results generated using the proposed geometric Bayesian model to those when a Dirichlet process prior is used.

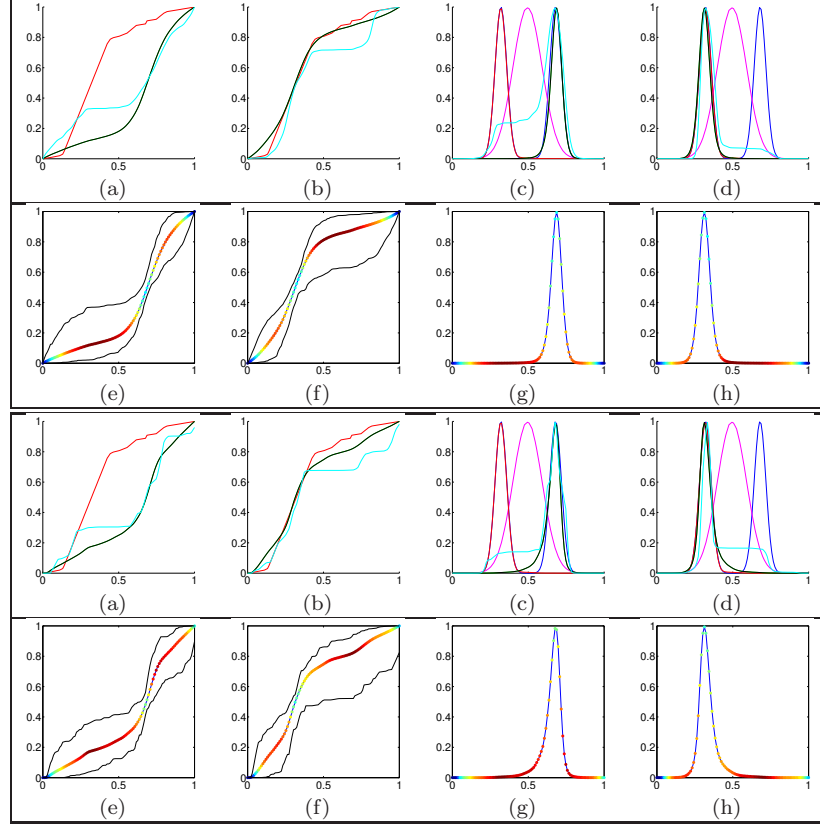


FIG 2. *Top: Results for the proposed model. Bottom: Results for model with Dirichlet process prior. (a)-(b) Summary for clusters 1 and 2, respectively: γ_{DP} (red), $\bar{\gamma}$ (green), $\hat{\gamma}$ (black), γ_{MAP} (cyan). (c)-(d) Summary for clusters 1 and 2: f_1 (blue), f_2 (magenta), $f_2 \circ \bar{\gamma}$ (green), $f_2 \circ \hat{\gamma}$ (black), $f_2 \circ \gamma_{MAP}$ (cyan). (e)-(f) Point-wise standard deviation (hot colors correspond to higher values) plotted on $\bar{\gamma}$ and 95% credible interval in clusters 1 and 2. (g)-(h) Point-wise standard deviation (hot colors correspond to higher values) plotted on $f_2 \circ \bar{\gamma}$ in clusters 1 and 2.*

Simulated Data: In the first set of examples we consider simulated functions where the number of expected modes in the posterior distribution is obvious. In the first example, displayed in the top of Figure 2, we consider warping a function with one peak (f_2) to match a function with two peaks (f_1). We expect the posterior distribution to have two distinct modes, one centered at a warping function that aligns the peak on f_2 with the left peak on f_1 and the other centered at a warping function that aligns the peak on f_2 to the right peak on f_1 . This is indeed what we see from the posterior samples. There are two clear clusters of warping functions that align the peak on f_2 to each of the peaks on f_1 . The dynamic programming algorithm provides only a single alignment similar to the one in cluster 2. The mean and median of the posterior samples in

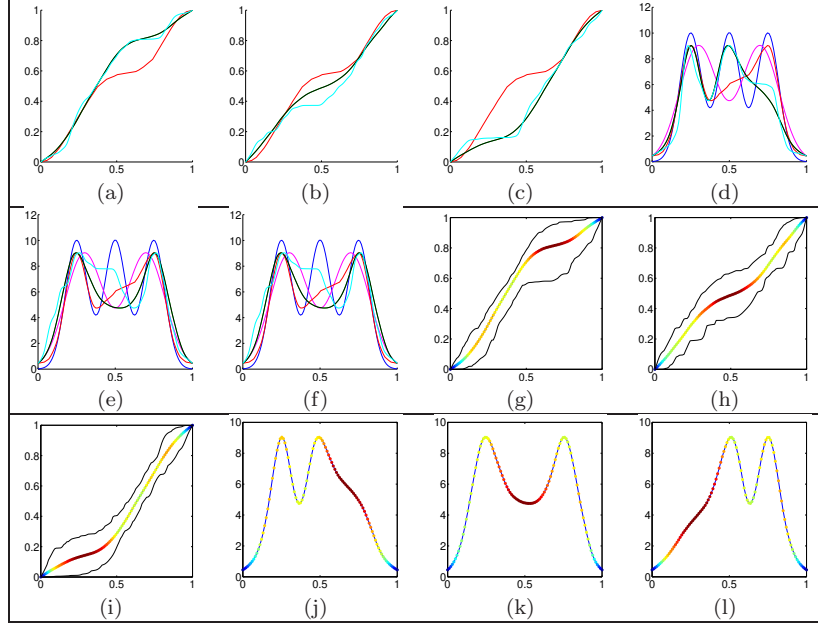


FIG 3. *Simulation results for the proposed model. (a)-(c) Summary for clusters 1, 2 and 3, respectively: γ_{DP} (red), $\tilde{\gamma}$ (green), $\tilde{\gamma}$ (black), γ_{MAP} (cyan). (d)-(f) Summary for clusters 1, 2 and 3: f_1 (blue), f_2 (magenta), $f_2 \circ \tilde{\gamma}$ (green), $f_2 \circ \tilde{\gamma}$ (black), $f_2 \circ \gamma_{MAP}$ (cyan). (g)-(i) Point-wise standard deviation (hot colors correspond to higher values) plotted on $\tilde{\gamma}$ and 95% credible interval in clusters 1, 2 and 3. (j)-(l) Point-wise standard deviation (hot colors correspond to higher values) plotted on $f_2 \circ \tilde{\gamma}$ in clusters 1, 2 and 3.*

each cluster are smoother than the DP result, although the function alignment seems very similar. The MAP estimate in each cluster prefers to spread the single peak on f_2 to match parts of both peaks on f_1 . The interesting result is that this type of alignment provides the smallest distance (1.3183, MAP estimate in cluster 1) between these two functions as computed using Equation 3, even smaller than the DP result (1.4255). While the DP algorithm could be adjusted to improve the estimation of the optimal warping function by making the discretization finer and increasing the search neighborhood, such refinements are not necessary in the proposed model. We also note that the uncertainty in alignment, as visualized using the colored standard deviation and the 95% credible interval, is highest where f_2 is constant. This happens because there are many possible alignments of such segments that do not adversely affect the quality of the global alignment. On the other hand, the alignment uncertainty is lowest at the peak of the function. We compare our results to those obtained when a Dirichlet process prior is used (bottom of Figure 2). While we are still able to find the two modes in the posterior, the MAP estimates are slightly worse than those provided by the proposed model (in terms of distance after alignment). This suggests that we are able to better explore the entire sample

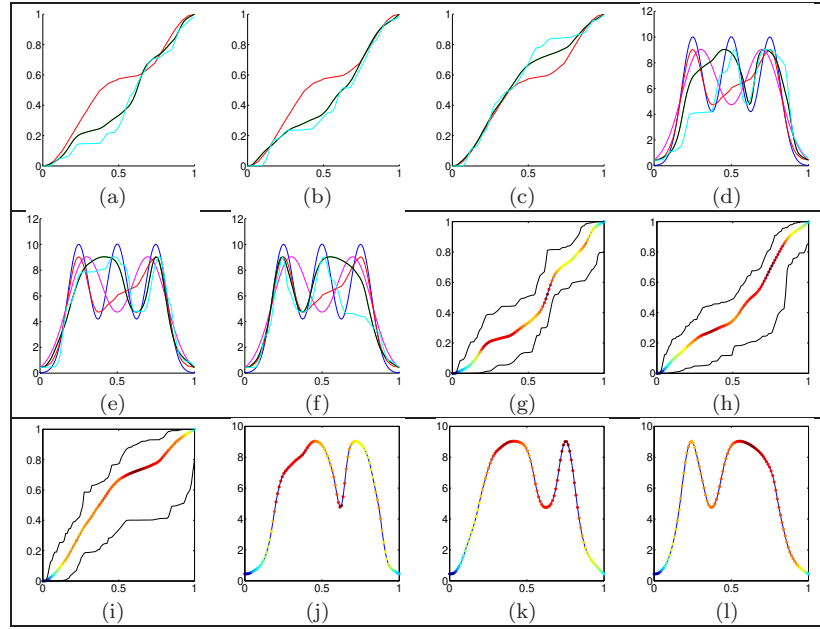


FIG 4. The same simulation results as in Figure 3 for the model with a Dirichlet process prior.

space. Also, the posterior mean and median warping functions in the two clusters do not provide as crisp of a match between f_1 and f_2 as those in the proposed model.

In the second example, displayed in Figures 3 and 4, we consider aligning a function with two peaks (f_2) to a function with three peaks (f_1). Here, we expect three modes in the posterior corresponding to the two peaks on f_2 aligning with the left and right, left and middle, and middle and right peaks on f_1 . This is what we see from the generated results. Again, the MAP estimate in cluster 1 provides a shorter distance between the warped functions (3.6350) than the DP algorithm (3.6615), although the difference here is much smaller. The alignment uncertainty, as in the previous example, is smallest around the peaks, which are the most prominent features in the two functions. Also, we notice that the model with the Dirichlet process prior (Figure 4) does not produce the three expected modes. In fact, clusters 1 and 2 are very similar and produce nearly the same alignment of the two functions.

Real Data: In Figures 5 and 6 we consider two real data examples using Berkeley growth data velocity curves and gene expression profiles, respectively. In the first example, we found that the posterior distribution has two modes. As one can see from the figures, the two clusters of warping functions provide realistic alignments but achieve them in different ways. The same can be seen in the gene expression data example, where three posterior modes were considered.

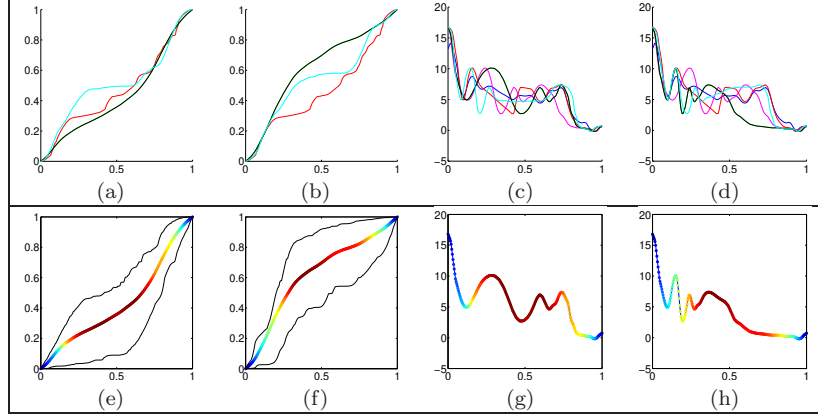


FIG 5. Results for Berkeley growth data velocity curves. (a)-(b) Summary for clusters 1 and 2, respectively: γ_{DP} (red), $\tilde{\gamma}$ (green), $\tilde{\gamma}$ (black), γ_{MAP} (cyan). (c)-(d) Summary for clusters 1 and 2: f_1 (blue), f_2 (magenta), $f_2 \circ \tilde{\gamma}$ (green), $f_2 \circ \tilde{\gamma}$ (black), $f_2 \circ \gamma_{MAP}$ (cyan). (e)-(f) Point-wise standard deviation (hot colors correspond to higher values) plotted on $\tilde{\gamma}$ and 95% credible interval in clusters 1 and 2. (g)-(h) Point-wise standard deviation (hot colors correspond to higher values) plotted on $f_2 \circ \tilde{\gamma}$ in clusters 1 and 2.

We note that it may be possible to split the displayed clusters into finer subgroups (representing more posterior modes). It is very difficult to establish the number of expected modes in the posterior of warping functions where real data is considered. We will further consider this problem in future work.

6. Function Alignment Using Maximum a Posteriori Probability (MAP) Estimate

In this section, we present various alignment results on simulated and real data using the maximum a posteriori probability estimate of the warping function. We use the MAP estimate in these cases because it provides a better solution when multiple modes are present. While in the previous section we were concerned with discovering multiple modes, here we are simply selecting one of the posterior samples to achieve the alignment. In each example, we compare the alignment achieved using the dynamic programming algorithm (Equation 2) (γ_{DP} , red) and two different importance sampling strategies; the first one uses the MAP estimate when the importance function is centered at γ_{id} ($\gamma_{MAP,id}$, green) and the second uses the MAP estimate when the importance function is centered at the solution obtained using the dynamic programming algorithm ($\gamma_{MAP,DP}$, black).

Simulated Data: We begin with four different examples concerned with registering simulated functions. The results are presented in Figure 7. In almost all of the given examples we see that γ_{DP} and $\gamma_{MAP,DP}$ are quite similar. In Example 2, we see that $\gamma_{MAP,DP}$ is significantly different from the dynamic

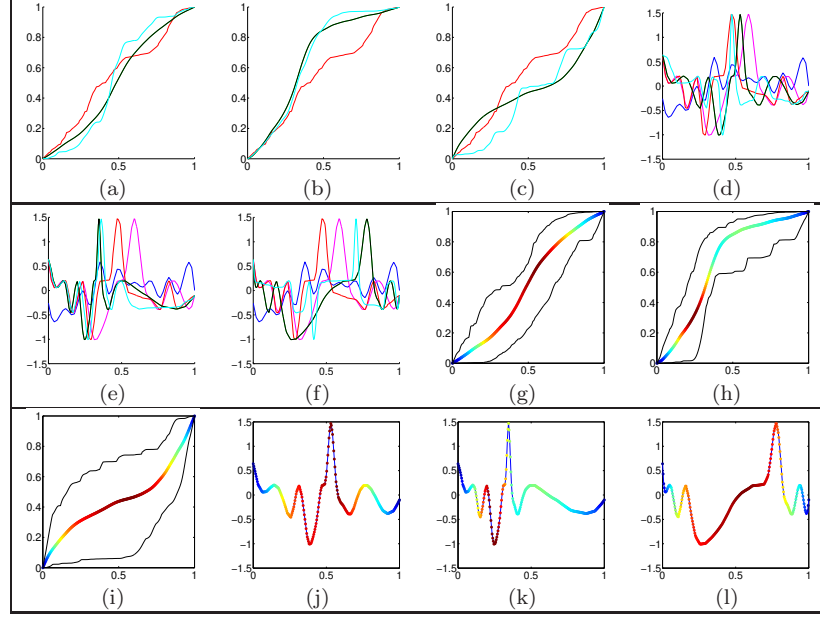


FIG 6. Results for gene expression data. (a)-(c) Summary for clusters 1, 2 and 3, respectively: γ_{DP} (red), $\tilde{\gamma}$ (green), $\tilde{\gamma}$ (black), γ_{MAP} (cyan). (d)-(f) Summary for clusters 1, 2 and 3: f_1 (blue), f_2 (magenta), $f_2 \circ \tilde{\gamma}$ (green), $f_2 \circ \tilde{\gamma}$ (black), $f_2 \circ \gamma_{MAP}$ (cyan). (g)-(i) Point-wise standard deviation (hot colors correspond to higher values) plotted on $\tilde{\gamma}$ and 95% credible interval in clusters 1, 2 and 3. (j)-(l) Point-wise standard deviation (hot colors correspond to higher values) plotted on $f_2 \circ \tilde{\gamma}$ in clusters 1, 2 and 3.

programming solution, and in fact, provides a better alignment based on the distance (reported in Table 1) between the registered functions. In most cases, the posterior variability is smaller when the dynamic programming solution is used as the mean of the importance function. Unfortunately, this may mean that this strategy has difficulty exploring the entire variable space as can be seen in Example 1. When the importance function is centered at the identity element of Γ one can see two clear modes (or clusters) in the posterior distribution. This is not as clear when the importance function is centered at the dynamic programming solution. Furthermore, the distance between registered functions is lowest when $\gamma_{MAP,id}$ is used for alignment. Finally, we emphasize that in all examples, the estimated alignment functions provide plausible yet different registrations.

Real Data: Here, we consider registration of functions arising in different real applications: gait and ECG biosignals, Berkley growth functions, gene expression and signature acceleration functions. The results are presented in Figure 8. Again, we note that the MAP estimates computed using the proposed Bayesian model perform well in all cases. While the distances between registered functions are almost always smaller when γ_{DP} is used for alignment, the MAP estimates also perform well based on visual inspection and the distance calculations pro-

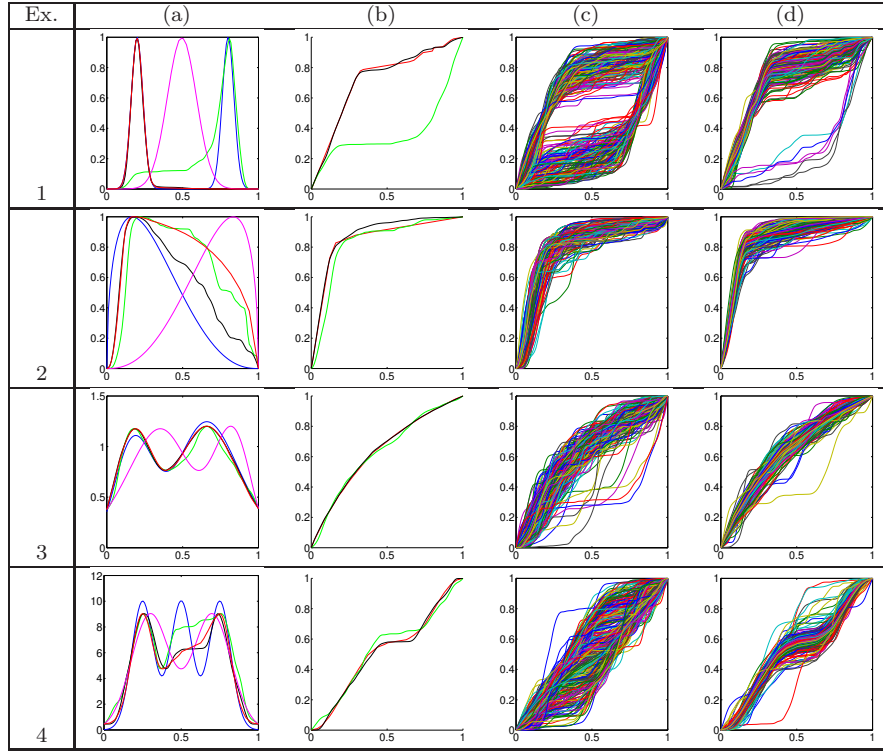


FIG 7. Bayesian registration of simulated data using MAP estimate of γ . (a) f_1 in blue, f_2 in magenta, $f_2 \circ \gamma_{DP}$ in red, $f_2 \circ \gamma_{MAP,id}$ in green, and $f_2 \circ \gamma_{MAP,DP}$ in black. (b) γ_{DP} in red, $\gamma_{MAP,id}$ in green, and $\gamma_{MAP,DP}$ in black. (c) Samples from posterior when importance sampling function has mean γ_{id} . (d) Samples from posterior when importance sampling function has mean γ_{DP} .

TABLE 1

Distances between functions after registration using various methods and importance sampling strategies for results displayed in Figure 7. Shortest distance is highlighted in bold.

Ex.	$\ q_1 - q_2\ $	$\ q_1 - (q_2, \gamma_{DP})\ $	$\ q_1 - (q_2, \gamma_{MAP,id})\ $	$\ q_1 - (q_2, \gamma_{MAP,DP})\ $
1	2.6668	1.4255	1.4043	1.4222
2	2.3387	1.0914	1.3232	0.8807
3	2.0753	0.0872	0.3615	0.1338
4	6.8599	3.6615	3.9022	3.5097

vided in Table 2. Additionally, the MAP estimates are always much smoother than the DP solution, which is desired in practice. The importance function centered at the solution of the dynamic programming algorithm again seems to have trouble exploring the entire variable space, especially in Example 5.

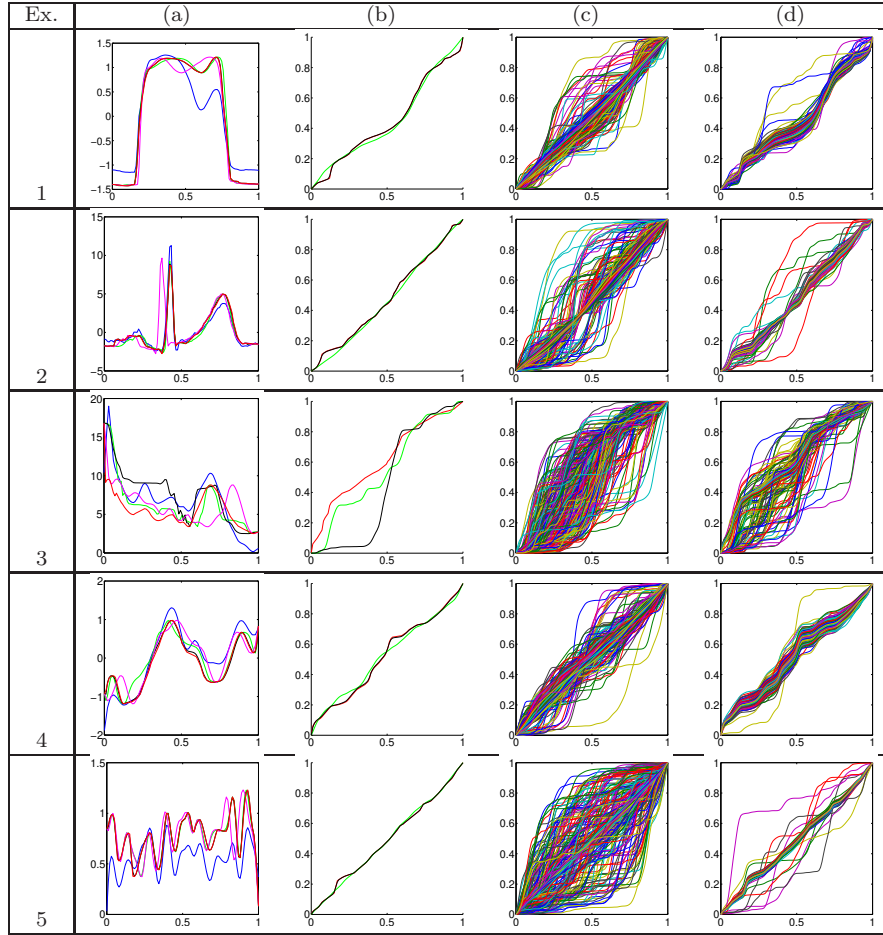


FIG 8. Bayesian registration of real data using MAP estimate of γ . Ex. 1: gait; Ex. 2: ECG PQRST complexes; Ex. 3: Berkley growth velocity; Ex. 4: Gene expression; Ex. 5: Signature acceleration data. (a) f_1 in blue, f_2 in magenta, $f_2 \circ \gamma_{DP}$ in red, $f_2 \circ \gamma_{MAP,id}$ in green, and $f_2 \circ \gamma_{MAP,DP}$ in black. (b) γ_{DP} in red, $\gamma_{MAP,id}$ in green, and $\gamma_{MAP,DP}$ in black. (c) Samples from posterior when importance sampling function has mean γ_{id} . (d) Samples from posterior when importance sampling function has mean γ_{DP} .

7. Summary and Future Work

We have presented a Bayesian model for pairwise registration of functional data. This model utilizes a convenient geometric representation of warping functions called the square-root density, which allows for efficient sampling from the posterior distribution via importance sampling. A main advantage of the proposed approach over previous energy based approaches is that it is possible to discover multiple plausible registrations, which are given by different modes in the posterior distribution. We present several simulated and real data examples that

TABLE 2
Distances between functions after registration using various methods and importance sampling strategies for results displayed in Figure 8. Shortest distance is highlighted in bold.

Ex.	$\ q_1 - q_2\ $	$\ q_1 - (q_2, \gamma_{DP})\ $	$\ q_1 - (q_2, \gamma_{MAP, id})\ $	$\ q_1 - (q_2, \gamma_{MAP, DP})\ $
1	1.9649	0.7302	1.0970	0.7363
2	8.9637	2.4153	3.1408	2.3644
3	9.3956	5.4187	5.2487	5.3750
4	2.7241	1.1033	1.8313	1.1940
5	2.8032	0.8396	1.4706	0.8439

highlight these advantages. We compare the results obtained using the proposed model to those obtained using a similar model with a Dirichlet process prior on the warping functions (which does not exploit the geometry of the space of warping functions).

In future work, we will extend these methods to a groupwise registration algorithm, where one is interested in aligning more than two functions simultaneously. Furthermore, we will extend these methods to a setting where soft landmark information is provided on the functions of interest. In such a case, one can incorporate this information into the prior distribution of the Bayesian model. Finally, we will consider a more general problem of curve alignment for shape analysis where the curves are functions from a unit interval (open curves) or unit circle (closed curves) to \mathbb{R}^n . Shapes of objects are invariant to translation, scale, rotation and re-parameterization and thus the prior distributions in our Bayesian model will be defined on product spaces, whose geometric structure will play an important role.

Acknowledgements

The author would like to thank Anuj Srivastava for useful suggestions and comments.

References

- [1] BHATTACHARYA, A. (1943). On a measure of divergence between two statistical populations defined by their probability distributions. *Bulletin of the Calcutta Mathematical Society* **35** 99-109.
- [2] CHENG, W., DRYDEN, I. L., HITCHCOCK, D. B., HUANG, X. and LE, H. (2013). Bayesian registration of functions and curves. *arXiv:1311.2105v1*.
- [3] DRYDEN, I. L. and MARDIA, K. V. (1998). *Statistical Shape Analysis*. John Wiley & Sons.
- [4] FLETCHER, P. T., VENKATASUBRAMANIAN, S. and JOSHI, S. (2009). The geometric median on Riemannian manifolds with application to robust atlas estimation. *Neuroimage* **45** S143-S152.
- [5] GERVINI, D. and GASSER, T. (2004). Self-Modeling Warping Functions. *Journal of the Royal Statistical Society, Series B* **66** 959-971.

- [6] JAMES, G. (2007). Curve Alignment by Moments. *Annals of Applied Statistics* **1** 480-501.
- [7] KNEIP, A. and GASSER, T. (1992). Statistical Tools to Analyze Data Representing a Sample of Curves. *Annals of Statistics* **20** 1266-1305.
- [8] KNEIP, A. and RAMSAY, J. O. (2008). Combining Registration and Fitting for Functional Models. *Journal of the American Statistical Association* **103** 1155-1165.
- [9] KURTEK, S., SRIVASTAVA, A., KLASSEN, E. and DING, Z. (2012). Statistical Modeling of Curves Using Shapes and Related Features. *Journal of the American Statistical Association* **107** 1152-1165.
- [10] KURTEK, S., SRIVASTAVA, A. and WU, W. (2011). Signal estimation under random time-warpings and nonlinear signal alignment. In *Neural Information Processing Systems (NIPS)* 675-683.
- [11] KURTEK, S., SU, J., GRIMM, C., VAUGHAN, M., SOWELL, R. T. and SRIVASTAVA, A. (2013). Statistical Analysis of Manual Segmentations of Structures in Medical Images. *Computer Vision and Image Understanding* **117** 1036-1050.
- [12] KURTEK, S., WU, W., CHRISTENSEN, G. E. and SRIVASTAVA, A. (2013). Segmentation, alignment and statistical analysis of biosignals with application to disease classification. *Journal of Applied Statistics* **40** 1270-1288.
- [13] LE, H. (2001). Locating Frechet Means with Application to Shape Spaces. *Advances in Applied Probability* **33** 324-338.
- [14] LIU, X. and MÜLLER, H. G. (2004). Functional convex averaging and synchronization for time-warped random curves. *Journal of the American Statistical Association* **99** 687-699.
- [15] MACQUEEN, J. B. (1967). Some Methods for Classification and Analysis of MultiVariate Observations. In *Fifth Berkeley Symposium on Mathematical Statistics and Probability* (L. M. L. CAM and J. NEYMAN, eds.) **1** 281-297.
- [16] RAMSAY, J. O. and LI, X. (1998). Curve Registration. *Journal of the Royal Statistical Society, Series B* **60** 351-363.
- [17] RAMSAY, J. O. and SILVERMAN, B. W. (2005). *Functional Data Analysis, Second Edition*. Springer Series in Statistics.
- [18] SRIVASTAVA, A., JERMYN, I. and JOSHI, S. H. (2007). Riemannian Analysis of Probability Density Functions with Applications in Vision. In *IEEE Conference on Computer Vision and Pattern Recognition* 1-8.
- [19] SRIVASTAVA, A., KLASSEN, E., JOSHI, S. H. and JERMYN, I. H. (2011). Shape Analysis of Elastic Curves in Euclidean Spaces. *IEEE Transactions on Pattern Analysis and Machine Intelligence* **33** 1415-1428.
- [20] SRIVASTAVA, A., WU, W., KURTEK, S., KLASSEN, E. and MARRON, J. S. (2011). Registration of Functional Data Using Fisher-Rao Metric. *arXiv:1103.3817v2*.
- [21] SUEMATSU, N. and HAYASHI, A. (2012). Time series alignment with Gaussian processes. In *IEEE International Conference on Pattern Recognition* 2355-2358.
- [22] TANG, R. and MÜLLER, H. G. (2008). Pairwise curve synchronization for functional data. *Biometrika* **95** 875-889.

- [23] TELESCA, D. and INOUE, L. Y. T. (2008). Bayesian hierarchical curve registration. *Journal of the American Statistical Association* **103** 328–339.
- [24] TELESCA, D., INOUE, L. Y. T., NEIRA, M., ETZIONI, R., GLEAVE, M. and NELSON, C. (2009). Differential Expression and Network Inferences through Functional Data Modeling. *Biometrics* **65** 793–804.
- [25] TSAI, T. H., TADESSE, M. G., WANG, Y. and RESSOM, H. W. (2013). Profile-Based LC-MS Data Alignment: A Bayesian Approach. *IEEE/ACM Transactions on Computational Biology and Bioinformatics* **99** 494–503.
- [26] TUCKER, J. D., WU, W. and SRIVASTAVA, A. (2013). Generative models for functional data using phase and amplitude separation. *Computational Statistics & Data Analysis* **61** 50–66.
- [27] TUCKER, J. D., WU, W. and SRIVASTAVA, A. (2014). Analysis of signals under compositional noise with applications to SONAR data. *IEEE Journal of Oceanic Engineering* **39** 318–330.
- [28] ČENCOV, N. N. (1982). *Statistical Decision Rules and Optimal Inferences. Translations of Mathematical Monographs* **53**. AMS, Providence, USA.
- [29] WU, W. and SRIVASTAVA, A. (2011). An information-geometric framework for statistical inferences in the neural spike train space. *Journal of Computational Neuroscience* **31** 725–748.